

# **Civil Engineering Journal**

(E-ISSN: 2476-3055; ISSN: 2676-6957)

Vol. 11, No. 09, September, 2025



# Nonlinear Inelastic Local Buckling Behavior of Steel Columns Subjected to Axial Compression

Phu-Cuong Nguyen <sup>1\*</sup>, Thanh-Tuan Tran <sup>1</sup>, Huy-Phuoc Nguyen <sup>1</sup>, Trung-Dung Tran <sup>1</sup>

<sup>1</sup> Advanced Structural Engineering Laboratory, Department of Structural Engineering, Faculty of Civil Engineering, Ho Chi Minh City Open University, Ho Chi Minh City, Vietnam.

Received 25 October 2024; Revised 29 July 2025; Accepted 11 August 2025; Published 01 September 2025

#### **Abstract**

This study develops a displacement-based finite element approach using one-element modeling to analyze the second-order inelastic local buckling of steel columns under axial compression. To account for local buckling, two new stress-strain relationships are proposed for steel using an energy method and assumptions from previous studies for both compact and slender cross-sections. Stress-strain curves of post-buckling regimes are modeled as nonlinear curves. Both geometric and material nonlinearity are considered in the buckling analysis. The effects of geometric nonlinearity are traced through stability functions. The tangent stiffness of steel members is continuously updated during the nonlinear analysis by updating the fiber behavior at monitoring cross-sections using the Gauss-Lobatto integration rule. The proposed stress-strain relationships accurately predict the ultimate strength, elastic, and inelastic local buckling behaviors of steel columns under axial compression, compared with ABAQUS and previous studies. The model accurately predicts elastic, inelastic, and ultimate strength behaviors, with post-buckling responses closely matching ABAQUS results (e.g. 0.881 (proposed with residual stress), 1.008 (proposed without residual stress) vs. 0.948 (ABAQUS) load ratio for HB3 specimen). This approach offers significant computational efficiency (~1.0 sec vs. 20–30 min for ABAQUS) and introduces adjustable constitutive models, enhancing practical design applications for steel structures. This study proves that the effects of residual stress on the local buckling cannot be ignored in the case of slender sections, since the differences of the ultimate load (with and without the initial residual stress) are equal to 63.3% for the HI4 specimen and 43.2% for the HS40-SH(B) specimen.

Keywords: Finite Element Method; Inelasticity; Local Buckling; Post-Buckling; Compact-Section and Slender-Section Stub Steel Columns.

## 1. Introduction

Steel is widely used in civil engineering because of its strength, ductility, and flexibility. However, buckling is an important issue and a weak point of steel structures. There are many types of buckling: local buckling, bending buckling, flexural torsional buckling, lateral-torsional buckling, etc. Several tests were investigated to observe the local buckling behavior of steel structures or steel-concrete composite structures [1-3]. Xue et al. [4] tested and simulated the local—overall buckling behavior of corroded H-section steel columns subjected to compression and bending simultaneously. Wu et al. [5] studied nonlinear stability of prestressed stayed I-section steel columns considering local buckling. Zhong et al. [6] studied local buckling of stainless steel stub columns with novel octagonal hollow sections. Han et al. [7] investigated the local-global buckling behaviour of axially compressive welded I-section steel columns including local corrosion. Some researchers investigated the local buckling effects of steel members or steel structures by employing numerical solutions based on various finite element methods [8-10]. Recently, Maity et al. [11] simulated the interactive buckling in steel members using a torsional fiber element

<sup>\*</sup> Corresponding author: cuong.pn@ou.edu.vn; henycuong@gmail.com



doi http://dx.doi.org/10.28991/CEJ-2025-011-09-022

© 2025 by the authors. Licensee C.E.J, Tehran, Iran. This article is an open access article distributed under the terms and conditions of the Creative Commons Attribution (CC-BY) license (http://creativecommons.org/licenses/by/4.0/).

integrated with a multiaxial local buckling constitutive model. Heredia Rosa et al. [12] developed a multiaxial plasticity model with softening for simulating inelastic cyclic local buckling in steel beam-columns. In this study, we try to propose a beam-column finite element method using the modeling of one element per beam-column member for investigating steel columns under local buckling.

Local buckling may occur before structures collapse, and then the collapsed load of steel structures is reduced. The local buckling mainly depends on slenderness, thickness, the shape of member sections, the member length, residual stresses, and initial imperfections. Nowadays, the local buckling phenomenon can be more easily investigated by employing finite element analysis commercial softwares (ABAQUS, ANSYS, ...) using types of plate, shell, or solid elements. Recently, Feng et al. [13] investigated 162 nonlinear finite element models of stainless steel hybrid K-joints with SHS-braces-to-CHS-chord using ABAQUS software, and they proposed design equations for predicting the strength of the K-joints. Roy et al. [14] analyzed the nonlinear behavior of cold-form built-up box sections using stainless steel material. Ananthi et al. [15] conducted experimental tests and simulated finite element analysis for cold-formed steel zed-section and hat-section columns applied axial compression. Local and distortional buckling behavior of aluminum alloy back-to-back channels, including web holes applied axial compression, was investigated by Fang et al. [16]. In the four mentioned studies, the authors efforted to use commercial software ABAQUS [17] to assess, modify, and validate the performance of the current design guidelines and also proposed new design guidelines. It is inefficient for computer sources and analysis time employing shell or solid elements for modeling.

In 1998, Uy [18] studied the local buckling of concrete-filled steel welded-box columns using experimental tests and a semi-analytical finite strip approach, considering the effects of concrete. Also in this study, the author developed the local buckling approach using the effective width concept. Local buckling using beam-column elements is unclearly evaluated through AISC-LRFD specification [19, 20] by using proposed equations from experimental tests or modifying the constitutive model of steel [21, 22]. The methods utilized for the modified stress-strain relationship are more accurate and rational than those based on experimental design equations, and they can easily capture nonlinear post-buckling responses of structures. Chan et al. [21] developed the modified stress-strain model for analyzing the large-deflection inelastic buckling behavior of square columns. The proposed method by Chan considers both residual stress and initial geometry imperfection. Chan's method can handle complex loading and boundary conditions, while it is difficult for other methods (such as the finite difference or the finite integral numerical scheme). Whereas, Skallerud & Amdahl [22, 23] developed a beam finite element model for tubular members considering the local inelastic buckling phenomenon. Beam elements are either based on integrating uniaxial stresses on the cross-section or plastic hinge approaches.

Thai et al. [10] modified the constitutive model of materials using the energy method to consider the local buckling. In their study, they used the flexibility-based fiber beam-column method invented by Neuenhofer & Filippou [24] to analyze nonlinear elastic problems and developed by De Souza [25] to analyze large-displacement inelastic problems. We see that modifying the constitutive model of materials is one of the suitable approaches for considering local buckling by energy methods. The proposed stress-strain relationships in this study are combined by linear lines and nonlinear curves, while those proposed by Chan et al. [21] and Skallerud & Amdahl [22] are combined by linear lines (tri-linear model). Concurrently, numerical simulations using finite element methods (FEM) have been employed to analyze local buckling utilizing commercial software like ABAQUS and ANSYS. However, these FEM models often rely on shell or solid elements, which can be computationally intensive and impractical for routine design and analysis, especially for large-scale structures.

In the literature, there is no study employing stability functions and combining the one-element modelling for predicting the local buckling. To address this gap, we will try to develop the research idea following this direction. In this study, a displacement-based finite element approach employing stability functions using one-element modeling for steel members is developed to include the effects of local buckling. Two new modified constitutive models for compact and slender steel sections are proposed in which a coefficient  $\alpha$  is used for permitting adjustment of the inelastic post-local buckling behavior. The generalized displacement control algorithm invented by Yang et al. [26] is implemented for predicting the behavior curves, including the nonlinear inelastic local buckling. The proposed procedure has illustrated the accuracy and efficiency of developed software through some examples.

# 2. Constitutive Model of Steel Materials Considering Local Buckling

Figure 1 illustrates the stress-strain relationships for steel elements for two types of sections (compact section and slender section) based on the energy method applied to plate steel. The geometry of these relationships depends on the sizes of steel elements, and a vital ratio is b/t, where b is the width and t is the thickness of cross-sections. It can be seen that compact sections obtain an ultimate strength higher than slender sections because slender sections are elastically buckled before steel material is yielded. The slender sections are assumed to collapse suddenly after obtaining the ultimate strength, while the compact sections are more stable due to the existence of the plastic strain regime before they collapse. The collapse of compact sections can be called to be due to inelastic buckling.

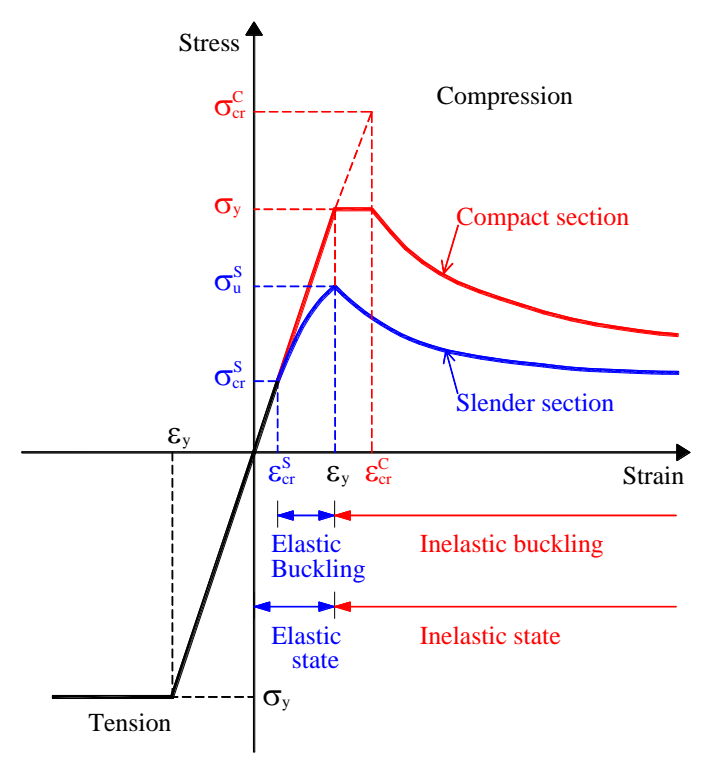


Figure 1. Stress-strain curves are assumed for steel elements

#### 2.1. Compact Sections

In this section, the formulation, including the effects of local buckling, is established by dividing cross-sections into some plate sections with the width b and the thickness t. Some assumptions are based on buckling theories of plate members. Considering plate sections, member sections with larger thickness, t, based on the ratio of width-to-thickness b/t, are compact sections. It is assumed that compact sections will yield before local buckling as illustrated in Figure 2. Elastic buckling stress  $\sigma_{cr}^{c}$  (C stands for Compact sections) is higher than yield stress  $\sigma_{y}$ . Figure 2 presents a new proposed modified stress-strain relationship of steel for considering inelastic local buckling for compact sections. The proposed stress-strain relationship is linear elastic-plastic with nonlinear softening. The linear elastic-plastic regime is defined by initial elastic modulus E, yield strain  $\varepsilon_{y}$ , yield stress  $\sigma_{y}$ , and elastic buckling strain  $\varepsilon_{cr}^{c}$ . The elastic buckling strain  $\varepsilon_{cr}^{c}$  is estimated by the elastic buckling stress  $\sigma_{cr}^{c}$  from the following formulas [27]:

$$\sigma_{cr}^{C} = \frac{\epsilon_{cr}^{C}}{E} = \frac{k\pi^{2}}{12(1-v^{2})(b/t)^{2}}$$
 (1)

in which k is the buckling parameter defined from boundary conditions of partioned plate sections found in Lee & Mahendran [28], and v is Poisson's ratio.

The elastic regime occurs when the stress-strain relationship of materials runs from point O to point A, as illustrated in Figure 2, corresponding to stress running from zero to the yield stress, and strain simultaneously runs from zero to the yield strain. The plastic regime starts from the point A and ends at the point B. It is noted that at point B, corresponding to the elastic buckling strain  $\varepsilon_{cr}^C$ , the monitoring plate will be buckled gradually. It is assumed that decreasing the cross-section area of a monitoring plate section due to inelastic local buckling is equivalent to decreasing strain energy due to inelastic local buckling. The inelastic local buckling curve can be predicted by utilizing a strain energy method for monitoring plates, as illustrated in Figure 2. The ratio of inelastic effective width and full width,  $b_{e'}b$  [18] or the ratio of current stress and yield stress  $b_e/b_y$  is equal to one minus the ratio of strain energy after inelastic local buckling and strain energy before inelastic local buckling  $\frac{U_A}{U_B}$ , presented as follows:

$$\frac{b_e}{b} \approx \frac{\sigma}{\sigma_V} = \frac{U_B - U_A}{U_B} = 1 - \frac{U_A}{U_B} \tag{2}$$

where  $U_B$  is the total strain energy created before point B (the point starts the inelastic local buckling),  $U_A$  is the total strain energy created after point B (the stress-strain relationship of materials will be softened nonlinearly), marked areas as shown in Figure 2, respectively, which are formulated as:

$$U_B^C = \frac{1}{2}\varepsilon_y \sigma_y + \left(\varepsilon_{cr}^C - \varepsilon_y\right) \sigma_y = \left(\varepsilon_{cr}^C - \frac{1}{2}\varepsilon_y\right) \sigma_y \tag{3}$$

$$U_A^C \approx \frac{1}{2} (\varepsilon - \varepsilon_{cr}^C) (\sigma_y + \sigma)$$
 (4)

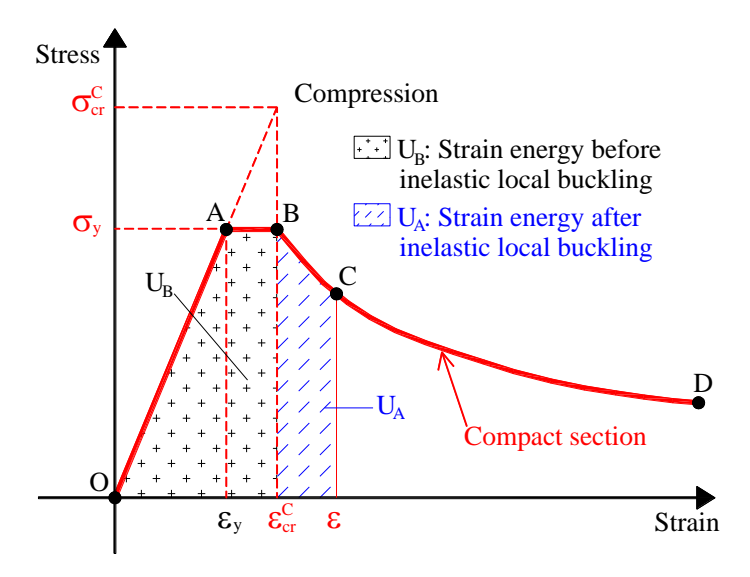


Figure 2. Stress-strain relationship of material and strain energy method for inelastic local buckling of compact sections

It is noted that the proposed Equations 3 and 4 in this study are quietly different from those of Thai et al. (2015) [10]. Thai and his colleagues used the total strain energy of the original constitutive model, neglecting the strain energy generated by the inelastic buckling regimes,  $U_I$ , and the strain energy generated by only the inelastic buckling regime. While Mursi & Uy (2004) [29] used the traditional stress-strain relationship of steel for calculating the total strain energies after or before inelastic local buckling, as shown in Figure 12 of their work.

Substituting Equations 3 and 4 into Equation 2, the inelastic post-local buckling stress is calculated approximately by the following formulas

$$\frac{\sigma}{\sigma_{y}} = \frac{1}{1 + \alpha \left(\frac{\varepsilon - \varepsilon_{CT}}{\varepsilon - \frac{\varepsilon_{Y}}{2}}\right)} \tag{5}$$

where  $\alpha$  is a coefficient for adjusting the inelastic post-local buckling curve.

From Equation 5, the tangent modulus of the material can be obtained as follows:

$$E_{t} = \frac{-\alpha \sigma_{y} \left(\varepsilon_{cr} - \frac{\varepsilon_{y}}{2}\right)}{\left((1+\alpha)\varepsilon - \frac{\varepsilon_{y}}{2} - \alpha\varepsilon_{cr}\right)^{2}} \tag{6}$$

In this study, the coefficient  $\alpha$  is assigned equal to 1.0 since the predicted results agree well with other studies (ABAQUS and Thai et al. [10]). So the inelastic post-local buckling stress and tangent modulus of steel are simplified as:

$$\frac{\sigma}{\sigma_{y}} = \frac{1}{1 + \left(\frac{\varepsilon - \varepsilon_{Cr}}{\varepsilon - \frac{\varepsilon_{y}}{2}}\right)} \tag{7}$$

$$E_t = \frac{-\sigma_y(\varepsilon_{cr} - \frac{\varepsilon_y}{2})}{\left(2\varepsilon - \frac{\varepsilon_y}{2} - \varepsilon_{cr}\right)^2} \tag{8}$$

in which  $E_t$  is the negative tangent modulus on the softening buckling curve.

# 2.2. Slender Sections

Considering thin-plate sections, member sections with smaller thicknesses, t, based on the width-to-thickness ratio (b/t is larger), are slender sections. Slender sections will be buckled suddenly without material yielding. Elastic buckling stress  $\sigma_{cr}^S$  (S stands for Slender sections), calculated by Equation 1, is lower than the elastic-ultimate buckling stress  $\sigma_u^S$  and more lower than yield stress  $\sigma_y$  of cross-sections. In this study, It is assumed that if  $\varepsilon_{cr} \leq \varepsilon_y$ , the partioned cross-section is the slender section so the stress-strain relationship of steel is described as Figure 3, otherwise, if  $\varepsilon_{cr} > \varepsilon_y$ , the partioned cross-section is the compact section so the stress-strain relationship of steel is described as Figure 2. Figure 3 presents a new proposed modified stress-strain relationship of steel for considering inelastic local buckling for slender sections. The proposed stress-strain relationship is linear elastic from point O to point A, nonlinear elastic from point A to point B, and nonlinear softening from the point B to point D. The linear-elastic nonlinear-elastic regime OAB is defined by initial Young's modulus E, elastic buckling stress  $\sigma_{cr}^S$ , elastic buckling strain  $\varepsilon_{cr}^S$ , yield strain  $\varepsilon_y$ , and elasticultimate buckling stress  $\sigma_u^S$ . It is essential to assume that elastic-ultimate buckling stress  $\sigma_u^S$  will occur at point B, corresponding to the yield strain  $\varepsilon_y$  of cross-sections.

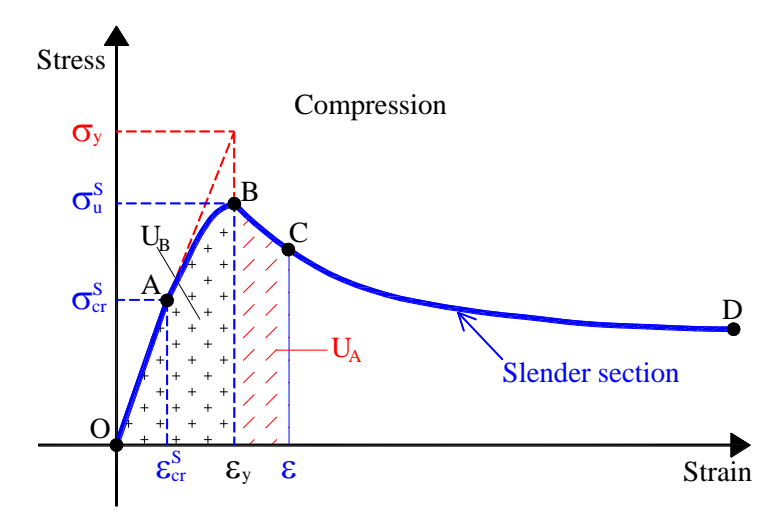


Figure 3. Stress-strain relationship of material and strain energy method for elastic local buckling of slender sections

The elastic-ultimate buckling stress  $\sigma_u^S$  is predicted by the effective width approach for a plate [18]. The elastic buckling formulation in Equation 1 can be applied by replacing elastic buckling stress  $\sigma_{cr}$  with yield stress  $\sigma_y$ , replacing the width b with the effective width  $b_e$ , and replacing the elastic buckling strain  $\varepsilon_{cr}$  with the yield strain  $\varepsilon_y$ . The yield strain can be estimated from Equation 1 as follows:

$$\varepsilon_{y} = \frac{\sigma_{y}}{E} = \frac{k\pi^{2}}{12(1-v^{2})(b_{e}/t)^{2}} \tag{9}$$

By using Equations 2 and 9, the elastic-ultimate buckling stress  $\sigma_u^s$  is estimated as follows:

$$\frac{\sigma_u^S}{\sigma_y} \approx \frac{b_e}{b} \tag{10}$$

$$\frac{\sigma_{cr}^{S}}{\sigma_{y}} = \left(\frac{b_{e}}{b}\right)^{2} \Rightarrow \frac{b_{e}}{b} = \sqrt{\frac{\sigma_{cr}^{S}}{\sigma_{y}}} \tag{11}$$

Combining Equations 10 and 11, we obtain the ultimate elastic buckling stress  $\sigma_u^S$  as follows:

$$\sigma_u^S = \sqrt{\sigma_{cr}^S \sigma_y} = E \sqrt{\varepsilon_{cr}^S \varepsilon_y} \tag{12}$$

Equation 12 is applied to predict the ultimate elastic buckling stress  $\sigma_u^S$  assumed at the yield strain  $\varepsilon_y$  at point B, as illustrated in Figure 3. The stress  $\sigma$  after elastic buckling at point A at the strain  $\varepsilon$  which is larger than the elastic buckling strain  $\varepsilon_{cr}^S$ , and smaller the yield strain  $\varepsilon_y$  (curve AB in Figure 3) can be estimated from Equation 12 by replacing  $(\sigma_u^S, \varepsilon_y)$  by  $(\sigma, \varepsilon)$ . We obtain Equation 13 as follows:

$$\sigma = E\sqrt{\varepsilon_{cr}^S \varepsilon}$$
 (13)

Diving both sides of Equation 13 to the yield stress  $\sigma_{\nu}$ , we obtain the following expression:

$$\frac{\sigma}{\sigma_{y}} = \frac{\sqrt{\varepsilon_{cr}^{S} \varepsilon}}{\varepsilon_{y}} \tag{14}$$

Equation 14 is used to estimate the stress in the nonlinear elastic regime from point A to point B.

From Equation 13, the tangent modulus of material in the nonlinear elastic regime AB can be obtained as follows:

$$E_t = \frac{E}{2} \sqrt{\frac{\varepsilon_{cr}^S}{\varepsilon}} \tag{15}$$

The stress-strain relationship after the ultimate elastic local buckling for slender sections is formulated by the above strain energy approach defined as follows:

$$\frac{\sigma}{\sigma_y} = \frac{\sqrt{\frac{\varepsilon_{Cr}^S}{\varepsilon_{y}}}}{1 + \alpha \left(1 - \frac{\varepsilon_{y}}{\varepsilon}\right)} \tag{16}$$

where  $\alpha$  is a coefficient for adjusting the elastic-ultimate post-local buckling curve.

The tangent modulus of the material is predicted by Equation 17 as follows:

$$E_{t} = \frac{-\sigma_{y} \left( \alpha \frac{\sqrt{\varepsilon_{CT}^{S} \varepsilon_{y}}}{\varepsilon^{2}} \right)}{\left( 1 + \alpha \left( 1 - \frac{\varepsilon_{y}}{\varepsilon} \right) \right)^{2}}$$

$$(17)$$

In this study, the coefficient  $\alpha$  is assigned equal to 1.0 since the obtained calculation agrees well with another study in the literature. So that the elastic-ultimate post-local buckling stress and tangent modulus of material are simplified as:

$$\frac{\sigma}{\sigma_y} = \frac{\sqrt{\frac{\varepsilon_{CT}^S}{\varepsilon_y}}}{2^{-\frac{\varepsilon_y}{\varepsilon}}} \tag{18}$$

$$E_t = \frac{-\sigma_y \sqrt{\varepsilon_{cr}^S \varepsilon_y}}{\left(2\varepsilon - \varepsilon_y\right)^2} \tag{19}$$

It can be noted that Equation 18 developed in this study is simpler than Equation 23 proposed in the work of Thai et al. [10].

## 3. Nonlinear Fiber Beam-Column Element

## 3.1. Considerations of P-δ and Shear Deformation

P- $\delta$  phenomenon is a phenomenon that the axial force acts on bending moments within members, and under an ultimate axial force, a structural member can be buckled suddenly. The P- $\delta$  phenomenon is usually considered by dividing beam-column members into several small elements. A number of sub-elements should be larger than ten elements (depending on the specify problems) for obtaining accurate predictions. For saving computational time and computer sources, stability functions [30] can be applied to develop a practical finite element analysis aiming to solve this local buckling problem because by using stability functions, the one-element model is utilized for predicting the P- $\delta$  effects accurately. Stability functions are successfully used through the works of Nguyen & Kim [31-36] for analyzing the nonlinear inelastic responses of space steel-framed structures with and without flexible beam-to-column joints under various actions. Stability functions are written by the Equations 25 and 26. Equation 20 represents the combination impacts of both the P- $\delta$  effect and shear deformation acting on a beam-column member

$$\begin{pmatrix} \Delta P \\ \Delta M_{yA} \\ \Delta M_{zA} \\ \Delta M_{zB} \\ \Delta T \end{pmatrix} = \begin{bmatrix} \frac{E_t A}{L} & 0 & 0 & 0 & 0 & 0 \\ 0 & C_{Ay} & C_{By} & 0 & 0 & 0 \\ 0 & 0 & 0 & C_{Az} & C_{Bz} & 0 \\ 0 & C_{By} & C_{Ay} & 0 & 0 & 0 \\ 0 & 0 & 0 & C_{Bz} & C_{Az} & 0 \\ 0 & 0 & 0 & 0 & 0 & \frac{GI}{L} \end{bmatrix} \begin{pmatrix} \Delta \delta \\ \Delta \theta_{yA} \\ \Delta \theta_{zA} \\ \Delta \theta_{yB} \\ \Delta \theta_{zB} \\ \Delta \phi \end{pmatrix}$$
 (20)

where considering a beam-column member has two ends, A and B, as shown in Figure 4; the increment of axial force  $\Delta P$ ; the increment of bending moments  $\Delta M_{yA}$ ,  $\Delta M_{zA}$ ,  $\Delta M_{yB}$ , and  $\Delta M_{zB}$ ; and the increment of torsional moment  $\Delta T$ ; the axial displacement  $\Delta \delta$ ; the joint rotations  $\Delta \theta_{yA}$ ,  $\Delta \theta_{zA}$ ,  $\Delta \theta_{yB}$ , and  $\Delta \theta_{zB}$ ; and the twist angle  $\Delta \varphi$ ; the tangent modulus of materials C; the shear modulus C; the torsional constant C. The bending stiffness factors ( $C_{Ay}$ ,  $C_{Az}$ ,  $C_{By}$ , and  $C_{Bz}$ ) considering shear deformation can be calculated as:

$$C_{Ay} = \frac{l_{Ay}^2 - l_{By}^2 + l_{Ay} A_{Sz} GL}{2l_{Ay} + 2l_{By} + A_{Sz} GL}$$
(21)

$$C_{AZ} = \frac{l_{AZ}^2 - l_{BZ}^2 + l_{AZ} A_{SY} GL}{2l_{AZ} + 2l_{BZ} + A_{SY} GL}$$
(22)

$$C_{By} = \frac{-l_{Ay}^2 + l_{By}^2 + l_{By} A_{sz} GL}{2l_{Ay} + 2l_{By} + A_{sz} GL}$$
 (23)

$$C_{Bz} = \frac{-l_{Az}^2 + l_{Bz}^2 + l_{By} A_{sy} GL}{2l_{Az} + 2l_{Bz} + A_{sy} GL} \tag{24}$$

where  $l_{An} = F_{An}(E_t I_n/L)$  and  $l_{Bn} = F_{Bn}(E_t I_n/L)$ ; the axes y and z are signed by n;  $F_{An}$  and  $F_{Bn}$  are stability functions formulated as:

$$F_{An} = \begin{cases} \frac{k_n L \sin(k_n L) - (k_n L)^2 \cos(k_n L)}{2 - 2 \cos(k_n L) - k_n L \sin(k_n L)} & \text{if } P < 0\\ \frac{(k_n L)^2 \cos(k_n L) - k_n L \sin(k_n L)}{2 - 2 \cosh(k_n L) + k_n L \sin(k_n L)} & \text{if } P > 0 \end{cases}$$
(25)

$$F_{Bn} = \begin{cases} \frac{(k_n L)^2 - k_n L \sin(k_n L)}{2 - 2 \cos(k_n L) - k_n L \sin(k_n L)} & \text{if } P < 0\\ \frac{k_n L \sin(k_n L) - (k_n L)^2}{2 - 2 \cosh(k_n L) + k_n L \sinh(k_n L)} & \text{if } P > 0 \end{cases}$$
(26)

in which  $k_n^2 = \frac{|P|}{E_t I_n}$ . The axial  $E_t A$  and bending stiffnesses  $E_t I_n$  of the beam-column element are calculated as Nguyen and Kim [33, 34]:

$$E_{t}A = \sum_{i=1}^{s} w_{i} (\sum_{i=1}^{m} E_{ti}A_{i})_{i}$$
(27)

$$E_{t}I_{n} = \sum_{i=1}^{s} w_{i} \left[ \sum_{i=1}^{m} E_{ti} (A_{i}n_{i}^{2} + I_{ni}) \right]_{i}$$
(28)

where *i* is the order number of fibers; the fiber number of a cross-section m; the control sections s; the weight of Lobatto technique  $w_j$  at the cross-section j [37]; the tangent modulus  $E_{ti}$  of a fiber i; the area of a fiber  $A_i$ ; and the moments of inertia around y- and z-axis  $I_{ni}$ ;  $n_i$  stands for coordinates of the fiber following y- and z-axes as shown in Figure 4.

For nonlinear analysis, the tangent stiffness matrix of members is continuously updated and memoried step by step during the analysis processing. The Gauss-Lobatto integration rule [37] is employed for estimating the axial and bending stiffness of the member because this scheme permits monitoring accurately the ends of the member where the behavior and mechanical properties of materials are changed.

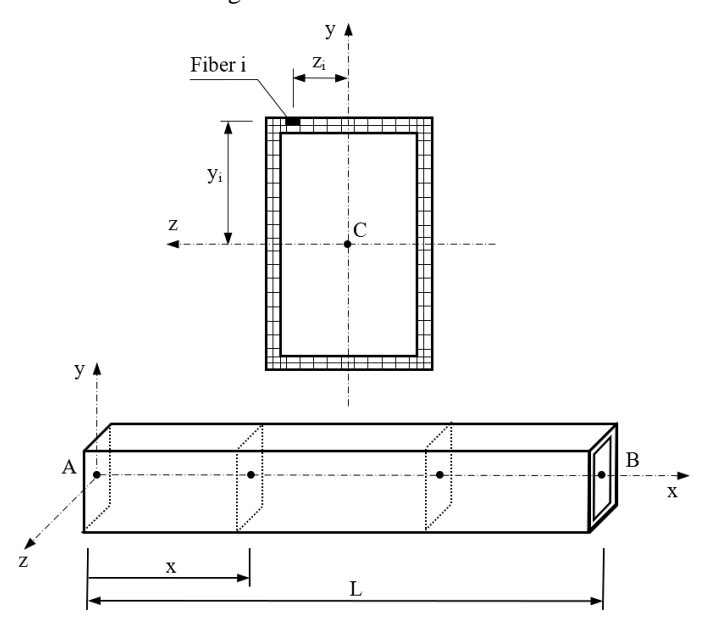


Figure 4. Modeling of a nonlinear beam-column element considering local buckling

#### 3.2. Updating the Elemental Stiffness Considering Local Buckling

In order to consider the effects of proposed steel constitutive models under axial force action, as illustrated in Figures 2 and 3, this research employs a beam-column finite element method based on dividing several fibers on the monitoring cross-sections that this method will be summarized here. The considered beam-column elements are monitored its behavior through integration points along the element length by applying Gauss-Lobatto integration rules [37]. At integration points, as shown in Figure 4, cross-sections are discretized into several fibers m with likely areas. These fibers have geometric characteristics, area  $A_i$ , and coordinate  $(y_i, z_i)$ , and they are saved and updated the behavior history of fibers, including stress, strain, and elastic modulus, during the analysis procedure. Initial residual stress is directly calculated by assigning initial stress for fibers at the first step of the analysis procedure, assuming that residual stresses distribute ideally as reference of Uy [18] for hollow-box sections and as Kitipornchai & Wong-Chung [38] for I-shape sections as presented in Figure 5.

The fiber-based approach inherently supports variations in residual stress distribution across different cross-section shapes. By discretizing the cross-section into fibers, the model allows for the assignment of distinct residual stress patterns tailored to specific geometries, such as box sections (Sections 4.1 and 4.3) and I-sections (Section 4.2). This flexibility enables the framework to accommodate arbitrary cross-section shapes by defining appropriate fiber layouts and corresponding residual stress distributions, ensuring applicability to a wide range of structural members in practical engineering design. Based on the fiber behavior, characteristics of monitoring sections (sectional stiffness matrix, sectional deformation, sectional force) are updated and evaluated, and then the member characteristics, including tangent stiffness matrix, member forces, etc., are also updated and evaluated for the next analysis step. The elemental tangent stiffness matrix is estimated and updated based on the fiber behavior through the tangent modulus of each fiber

depending on the proposed stress-strain relationship as presented in Figure 2, Equation 8 and Figure 3., Equation 15, Equation 19. For compact sections as illustrated in Figure 2, the tangent modulus of fiber is equal to Young's modulus (elastic regime, OA) if the fiber strain ranges from 0 to  $\varepsilon_y$ , the tangent modulus of fiber is equal to zero due to the fiber is yielding (plastic regime, AB) if the fiber strain ranges from  $\varepsilon_y$  to  $\varepsilon_{cr}^C$ , the tangent modulus of fiber will be estimated by the Equation 8 (softening regime, BD, post inelastic local buckling) if the fiber strain ranges from  $\varepsilon_{cr}^C$  to defined value. For slender sections, as shown in Figure 3, the tangent modulus of fiber is equal to Young's modulus (elastic regime, OA) if the fiber strain ranges from 0 to  $\varepsilon_{cr}^S$ , the tangent modulus of fiber will be estimated by the Equation 15 (elastic local buckling regime, AB) if the fiber strain ranges from  $\varepsilon_{cr}^S$  to  $\varepsilon_y$ , the tangent modulus of fiber will be estimated by the Equation 19 (softening regime, BD, post ultimate-elastic local buckling) if the fiber strain ranges from  $\varepsilon_y$  to defined value. The detailed nonlinear fiber beam-column finite element formulations developed by Nguyen & Kim [33, 34] are applied for proposing the nonlinear inelastic local buckling responses of steel columns in this study. When the tangent modulus of fibers is updated, axial and bending stiffness of member is also updated by the Equation 27 to 28, and the *j*-section stiffness matrix  $\left[k_{sec}^j\right]$  is calculated as follows:

$$\begin{bmatrix} k_{sec}^{j} \end{bmatrix} = \begin{bmatrix} \sum_{i=1}^{m} E_{ti} A_{i} & \sum_{i=1}^{m} E_{ti} A_{i} z_{i} & -\sum_{i=1}^{m} E_{ti} A_{i} y_{i} \\ \sum_{i=1}^{m} E_{ti} A_{i} z_{i} & \sum_{i=1}^{m} E_{ti} \left( A_{i} z_{i}^{2} + I_{yi} \right) & -\sum_{i=1}^{m} E_{ti} A_{i} z_{i} y_{i} \\ -\sum_{i=1}^{m} E_{ti} A_{i} y_{i} & -\sum_{i=1}^{m} E_{ti} A_{i} z_{i} y_{i} & \sum_{i=1}^{m} E_{ti} \left( A_{i} y_{i}^{2} + I_{zi} \right) \end{bmatrix}$$
(29)

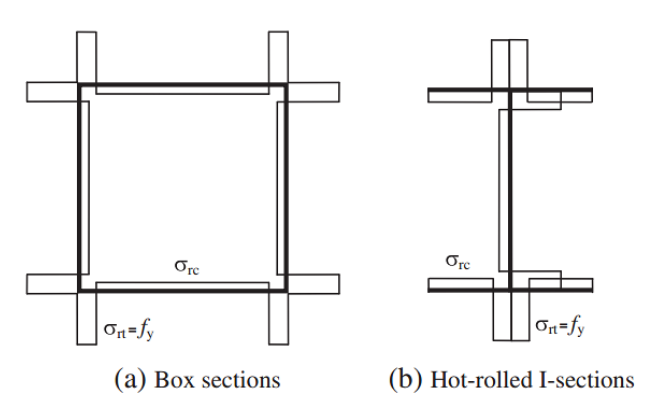


Figure 5. Idealized residual stress patterns

The incremental *j*-section force vectors  $\{\Delta Q^j\} = \{\Delta N^j \ \Delta M_y^j \ \Delta M_z^j\}^T$  at monitoring sections, are predicted by Nguyen and Kim [33, 34].

$$\{\Delta Q^j\} = [B(x)]\{\Delta F\} \tag{30}$$

$$[B(x)] = \begin{bmatrix} 1 & 0 & 0 & 0 & 0 & 0 \\ 0 & \frac{x}{L} - 1 & 0 & \frac{x}{L} & 0 & 0 \\ 0 & 0 & \frac{x}{L} - 1 & 0 & \frac{x}{L} & 0 \end{bmatrix}$$
(31)

where  $\{\Delta F\}$  is the incremental element force vector, [B(x)] is the interpolation matrix, and x is the coordinate of the j-section along the member length.

The incremental *j*-section deformation vectors  $\{\Delta q^j\} = \{\Delta \varepsilon^j \quad \Delta \chi^j_y \quad \Delta \chi^j_y\}^T$  are calculated as

$$\{\Delta q^{j}\} = [k_{sec}^{j}]^{-1} \{\Delta Q^{j}\}$$
(32)

where  $\Delta \varepsilon^j$  is the normal strain at the *j*-section, section stiffness  $\Delta \chi_y^j$  is the *y*-axis curvature strain at the *j*-section,  $\Delta \chi_z^j$  is the *z*-axis curvature strain at the *j*-section.

The incremental longitudinal *j*-section fiber strain vectors are estimated as:

$$\{\Delta e^j\} = [g]\{\Delta q^j\} \tag{33}$$

in which [g] is the fiber coordinate matrix present as:

$$[g] = \begin{bmatrix} 1 & z_1 & -y_1 \\ 1 & z_2 & -y_2 \\ \dots & \dots & \dots \\ 1 & z_m & -y_m \end{bmatrix}$$
(34)

As The incremental longitudinal *j*-section fiber strain vectors are calculated, the current fiber stresses are predicted using the proposed stress-strain relationships.

The resisting forces of the j-section are estimated as:

where  $\sigma_i$  is the normal stress at the *i*-fiber.

The tangent modulus of each fiber  $E_{ti}$  is estimated based on the stress-strain constitutive laws of material as Equations 8, 15 and 9. At each loop procedure, the elemental tangent stiffness matrix is estimated through updating the tangent elastic modulus of each fiber to take into accounting the effects of local buckling from two proposed stress-strain relationships (Figures 2 and 3). Figure 6 presents the flowchart for predicting the local buckling behavior through monitoring the behavior of steel fibers using the proposed stress-strain relationships.

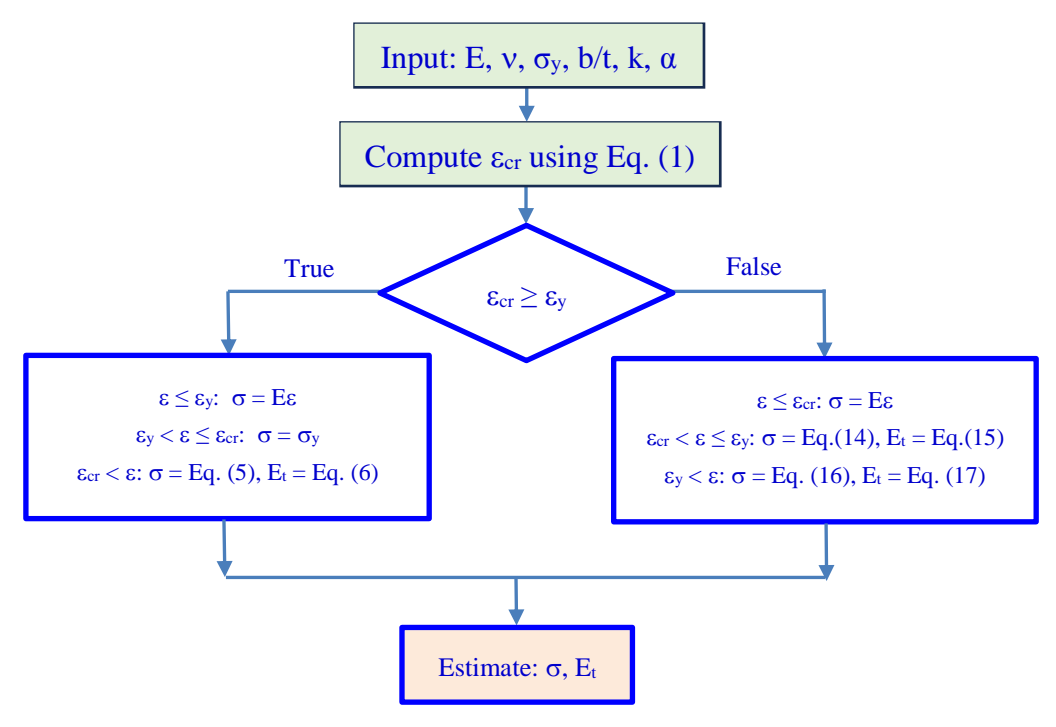


Figure 6. . Flowchart predicts the local buckling behavior through monitoring the behavior of steel fibers using the proposed stress-strain relationships

## 4. Numerical Examples

A FORTRAN program is coded using the proposed beam-column finite element procedure to trace the nonlinear inelastic local buckling response of steel members under axial compressive loadings. All numerical examples use modeling of one element for steel members, including five control points along the length of the member. Cross-sections of steel columns are meshed into 92 small fibers. The generalized displacement control algorithm invented by Yang et al. [26] is employed to develop the proposed program for capturing the local buckling behavior of structures.

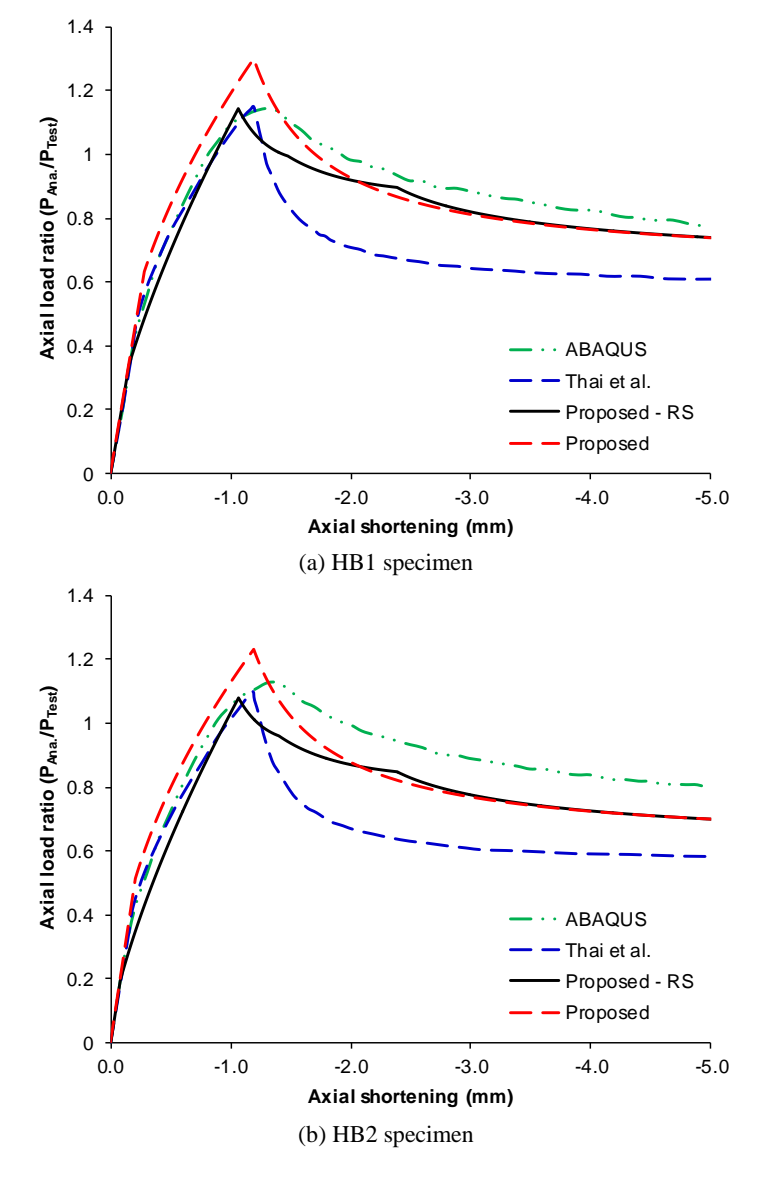
#### 4.1. Compression of Steel Box Stub Columns With Normal Strength

This example verifies the capacity of compression resistance of normal-strength-steel welded box-section stub columns. Uy [39] carried out four experimental tests for box sections with strengthening stiffeners. Mechanical characteristics of steel are E = 200000 MPa and  $\sigma_y = 265$  MPa. Initial compressive residual stresses measured by Uy [39] are 15% to 17% of the yield stress, as shown in Table 1. The geometry dimensions of steel columns are presented in Table 1.

Table 1. Geometry dimensions of steel box columns are studied

Specimens	b (cm)	t (cm)	b/t	A (cm <sup>2</sup> )	L (cm)	$\sigma_{\rm rc}/\sigma_{\rm y}$
HB1	36	0.3	120	42.84	90	0.16
HB2	42	0.3	140	50.04	90	0.17
HB3	48	0.3	160	57.24	90	0.15
HB4	54	0.3	180	64.44	90	0.15

The load ratio-axial shortening responses captured by the proposed program, ABAQUS [17] from Thai et al.'s work [10], and Thai et al. [10] are drawn respectively in Figure 7 for comparing the accuracy and reliability of this work. It is noted that the results of ABAQUS [17] presented in this study were summarized from Thai et al.'s work [10]. It is observed that the post-buckling behavior of the proposed method is closer to ABAQUS's one than Thai et al.'s result. As shown in Figure 7, all four specimens behave as slender sections, steel columns are buckled before steel fibers are yielded. The post-buckling path generated by the proposed method considering initial residual stresses is not as smooth as one without residual stresses due to the chances of tangent elastic modulus of each fiber with different stress-strain relationships. Because the tangent elastic modulus of all fibers is the same of value in the case without considering initial residual stresses, while the tangent elastic modulus of fibers is different depending on initial residual stresses in the remain case (Present with RS). In the case of the HB3 specimen, the peak compression load calculated by the presented method with effects of residual stress (Present with RS) is lower, about 14.42%, than the peak compression load calculated by the presented method without effects of residual stress (Present without RS). The range of difference between considering and no considering the residual stress obtained for four specimens is from 13.72% to 14.42%. Figure 7 illustrates that residual stresses are significant on the compressive behavior of box steel columns. Based on the proposed coefficient α, the proposed method can easily adjust the post-buckling path with the obtained results of commercial FEA software packages. In this example, the proposed coefficient α is equal to 1.0 used for analyzing. Table 2 shows the comparison of ultimate analytical and experimental compression load ratios of the proposed method, ABAQUS [17] from Thai et al.'s work [10], and Thai et al. [10]. The proposed method's ultimate load ratios for slender sections (HB1-HB4) range from 0.881 to 1.144, compared to ABAQUS's 0.948-1.149. The proposed method's predictions are within 2-7% of ABAQUS for HB1, HB2, and HB4, but deviate by ~7% for HB3 (0.881 vs. 0.948). Figure 7 shows that the proposed method's post-buckling curves closely align with ABAQUS for HB1 and HB2, indicating the reliable prediction of post-buckling strength. The proposed method's post-buckling curves are better than those of Thai et al. [10]. It is noted that ABAQUS from Thai et al.'s work [10] used 1200 shell elements for the calculation considering initial geometry imperfections and residual stress, while Thai et al. [10] applied the flexibilitybased fiber finite element method invented by Neuenhofer & Filippou [24] and improved by De Souza [25] for their analyses. The present method does not consider initial geometry imperfections.



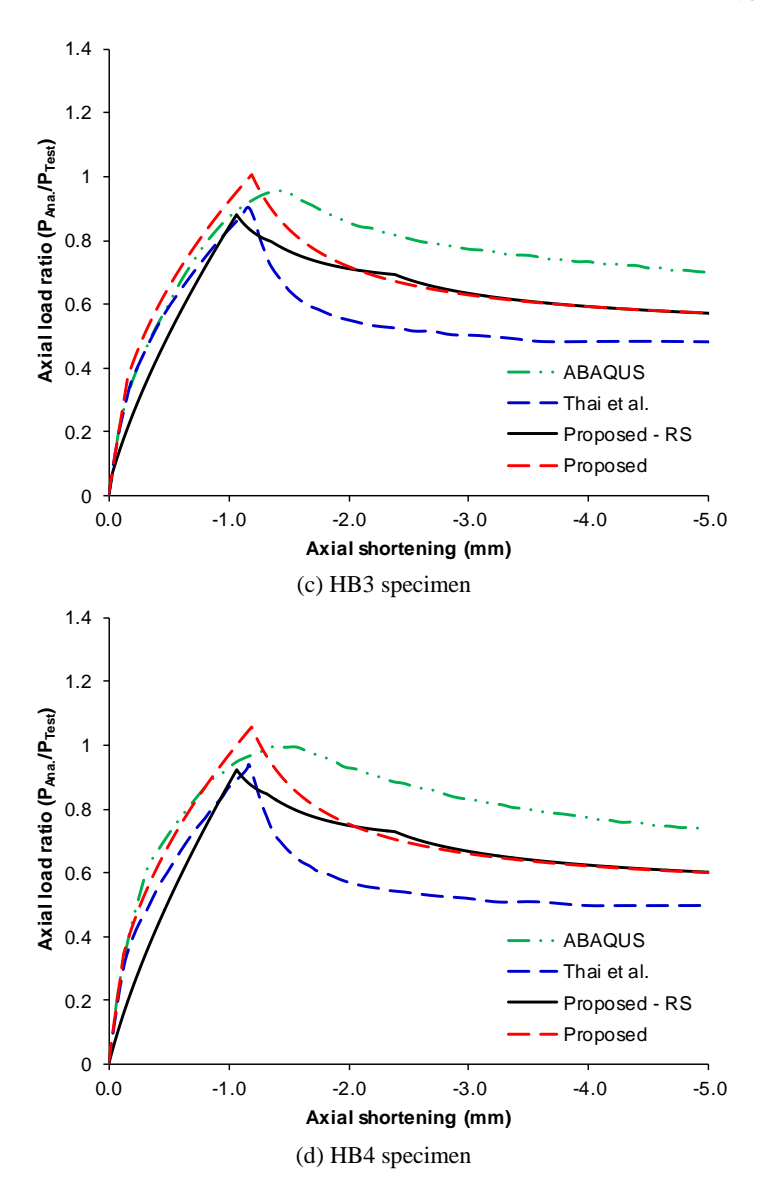


Figure 7. Load ratio-axial shortening curves of steel box stub columns with normal strength

Table 2. Comparison of ultimate compression load ratios for steel box specimens

Specimens	P <sub>Test</sub> (kN)	P <sub>Ana</sub> /P <sub>Test</sub>					
	[39]	ABAQUS [10]	Thai [10]	Present (with RS)	Present (without RS)		
HB1	425	1.149	1.149	1.144	1.301		
HB2	450	1.123	1.094	1.080	1.230		
HB3	550	0.948	0.895	0.881	1.008		
HB4	525	0.996	0.937	0.924	1.056		

The solution time for the problem using the proposed program is about 1.0 sec using the suggested beam-column element running on a HP laptop computer configuration of Intel Core i7-7500U, 16 GB RAM, and Windows 10 Home 64-bit. In contrast, ABAQUS simulations with 1200–2000 shell elements, as used in Thai et al. [10], are estimated to take approximately 20–30 minutes on comparable hardware, highlighting the significant computational efficiency of the proposed method.

## 4.2. Compression of Steel I-Section Stub Columns with Normal Strength

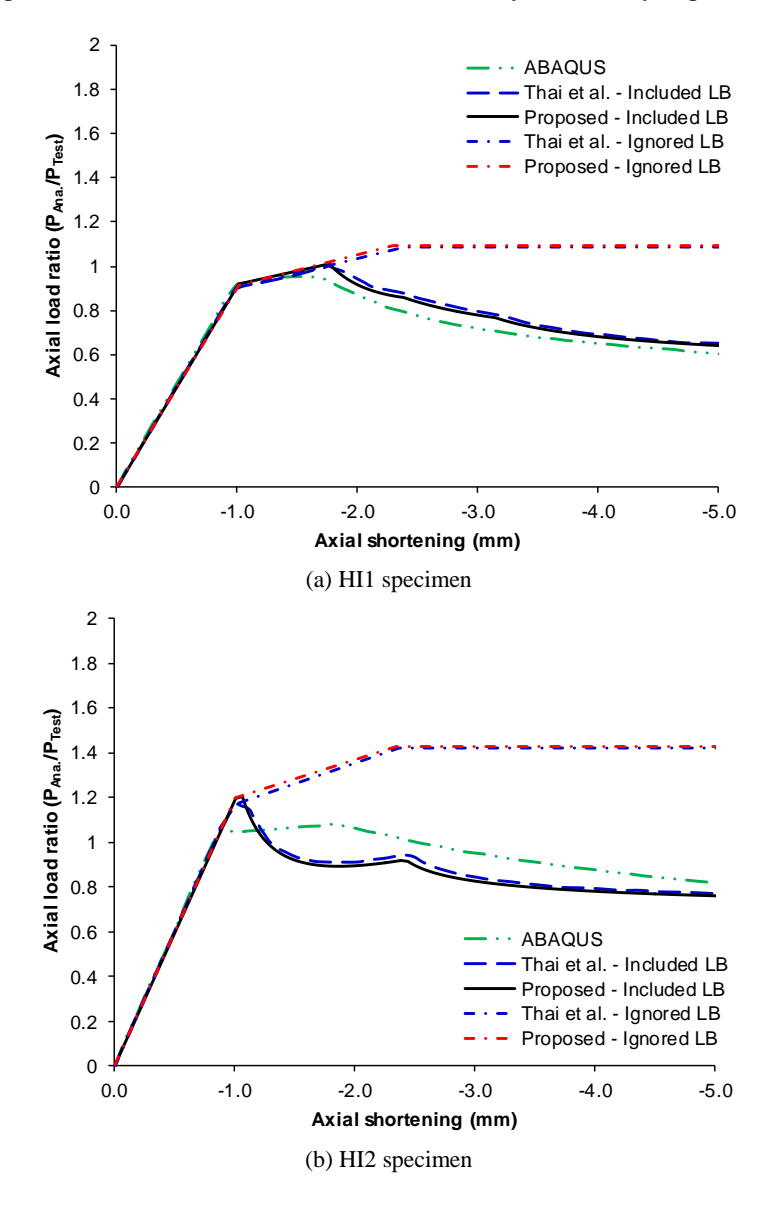
This example verifies the compressive resistance capacity of normal-strength steel welded I-section stub columns. Uy [39] carried out four experimental tests of I-sections with stiffeners. Mechanical properties of steel are E = 200000 MPa and  $\sigma_y = 265$  MPa. The width-to-thickness ratio (b/t) of columns was varied from 20 to 35. Initial compressive residual stresses studied by Uy [39] are equal to 17% to 19% of the yield stress, as shown in Table 3. Geometry

dimensions and initial compressive residual stresses of all columns are illustrated in Table 3. That et al. [10] analyzed the behavior of these specimens using initial compressive residual stresses of 18%, while we assigned initial residual stresses for 92 fibers as presented in Figure 5-b and Table 3.

Table 3. Geometry dimensions of steel I-section specimens are studied

Specimens	b (cm)	t (cm)	b/t	A (cm <sup>2</sup> )	L (cm)	$\sigma_{rc}/\sigma_{y}$
HI1	6.0	0.3	20	10.62	90	0.18
HI2	7.5	0.3	25	13.32	90	0.19
HI3	9.0	0.3	30	16.02	90	0.18
HI4	10.5	0.3	35	18.72	90	0.17

Figure 8 illustrated the load-axial displacement behavior considering local buckling solved by the presented program, ABAQUS [10], and Thai et al. [10]. It is seen that the curves obtained by the presented method match well with those of Thai et al. [10]. The limit load calculated by the presented program is higher slightly than the result estimated by Thai et al.'s program. As shown in Figure 8, HI1 and HI2 specimens behave as compact sections, while HI3 and HI4 specimens behave as slender sections. Table 4 presented a list of ultimate compression load ratios calculated from the proposed method, ABAQUS [10], and Thai et al. [10]. The proposed method yields load ratios of 1.011–1.205 for HI1–HI4, compared to ABAQUS's 0.949–1.082. The model accurately predicts post-buckling behavior for compact sections (HI1–HI2), with load ratios within 6% of ABAQUS, but over predicts by 6–12% for slender sections (HI3–HI4). Figure 8 confirms good agreement in post-buckling paths for HI1–HI2, with slight deviations for HI3–HI4. For the HI4 specimen, the ultimate load differs significantly when considering the effects of local buckling and not considering. Local buckling is an important issue that needs to be evaluated carefully in the analysis procedure.



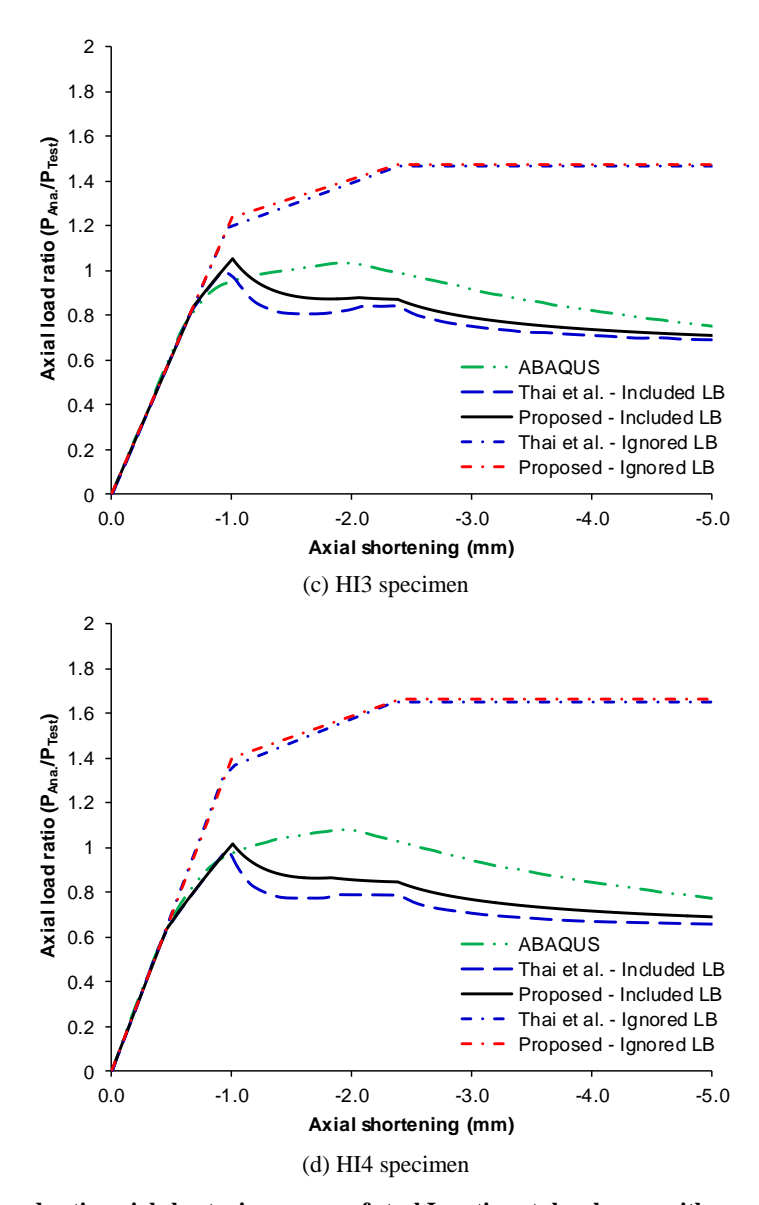


Figure 8. Load ratio-axial shortening curves of steel I-section stub columns with normal strength

Table 4. Comparison of ultimate compression load ratios for steel I-section specimens

Specimens	P <sub>Test</sub> (kN)	$\mathbf{P}_{\mathrm{Ana}}/\mathbf{P}_{\mathrm{Test}}$						
	[39]	ABAQUS [10]	Thai [10] (with LB)	Thai [10] (without LB)	Present (with LB)	Present (without LB)		
HI1	260	0.949	0.999	1.082	1.011	1.090		
HI2	250	1.075	1.168	1.412	1.205	1.427		
HI3	290	1.033	1.000	1.464	1.053	1.471		
HI4	300	1.082	0.997	1.654	1.017	1.661		

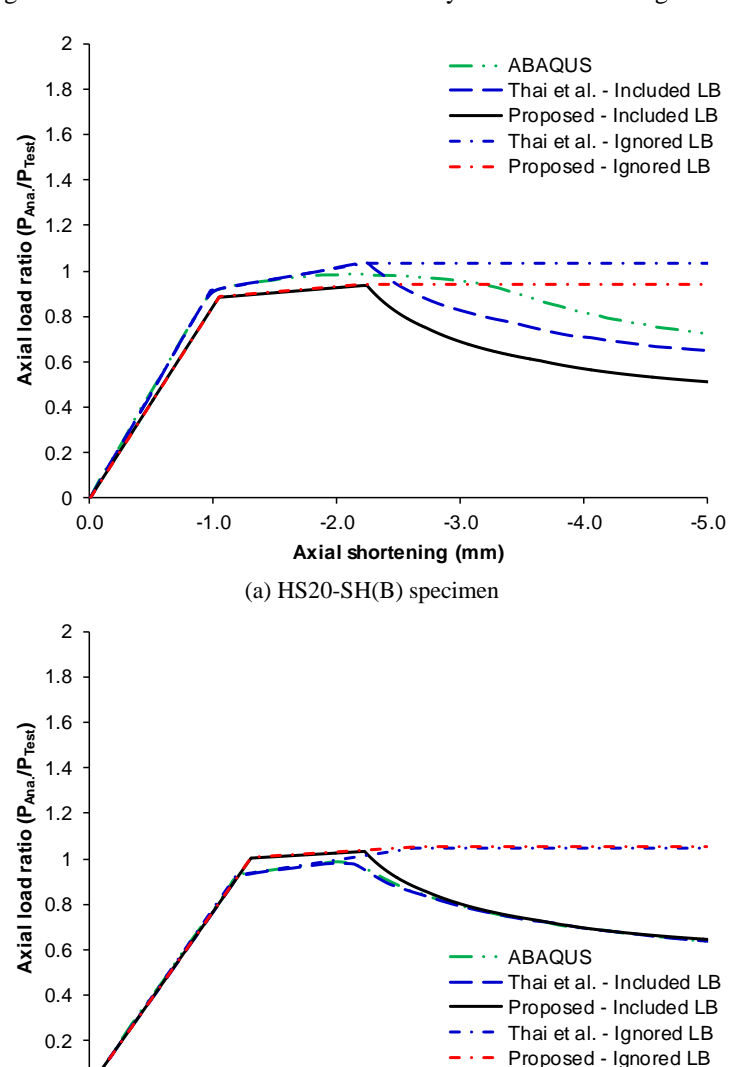
## 4.3. Compression of Steel Box Stub Columns with High Strength

This example performs the compressive behavior of high-strength steel welded box-section stub columns. Uy et al. [40] experimentally tested forty specimens of steel hollow-box sections with strengthening stiffeners under monotonic compressive loading for capturing local buckling responses of columns. The stub specimens have a width-to-thickness ratio (b/t) of 15 to 40. Steel plates's thickness of square-box sections are 5 mm. The yield strength of 760 MPa provided by tensile coupon tests is used in this analysis. Young's modulus is 220000 MPa. For verification, the dimensions and input data of all specimens analyzed by Thai et al. [10], as listed in Table 5, are also investigated in this study. It is important to note that Thai et al. [10] used four columns with a length-to-width ratio of 3.1, approximately, while the real experimental tests of Uy et al. [40] are 3.5.

Table 5. Geometry dimensions of high-strength steel box specimens are studied

Specimens	b (cm)	t (cm)	b/t	L (cm)	$\sigma_{\rm rc}/\sigma_{\rm y}$	$\sigma_{rt}/\sigma_{y}$
HS20-SH(B)	10.0	0.5	20	32.0	0.10	1.0
HS25-SH(B)	12.5	0.5	25	39.5	0.10	1.0
HS30-SH(B)	15.0	0.5	30	47.0	0.15	1.0
HS40-SH(B)	20.0	0.5	40	62.0	0.15	1.0

The results obtained by the presented program, ABAQUS [10], and Thai et al. [10] are illustrated and summarized in Figure 9 and Table 6, respectively. It is observed that the load-axial displacement curves obtained from the presented method are close to curves estimated by ABAQUS and Thai et al. HS20, HS25, and HS30 specimens are compact sections, while the HS40 specimen is a slender section, as shown in Figure 9. Only the HS40 specimen is buckled in the elastic regime due to a slender section with b/t = 40. Table 6 shows the comparison of ultimate analytical and experimental compression load ratios of the proposed method, ABAQUS [10], and Thai et al. [10]. The proposed method's load ratios range from 0.935 to 1.204 for HS20–HS40, compared to ABAQUS's 0.980–1.150. The proposed model performs well for compact sections (HS20–HS30), with differences of 4–5%, but over predicts by ~5% for the slender HS40 (1.204 vs. 1.150). Figure 9 shows close alignment of post-buckling curves for HS20–HS30, with minor deviations for HS40. Local buckling behaviors in the case of high-strength steel box stub columns (Figure 9) calculated by the presented method competed to results calculated from ABAQUS are more identical than the case of normal-strength steel I-section stub columns (Figure 8). The presented program can predict the nonlinear inelastic locally post-buckling and pre-buckling behavior of steel members with arbitrary sections and strength.



Axial shortening (mm)
(b) HS25-SH(B) specimen

-2.0

-3.0

-4.0

-5.0

0.0

-1.0

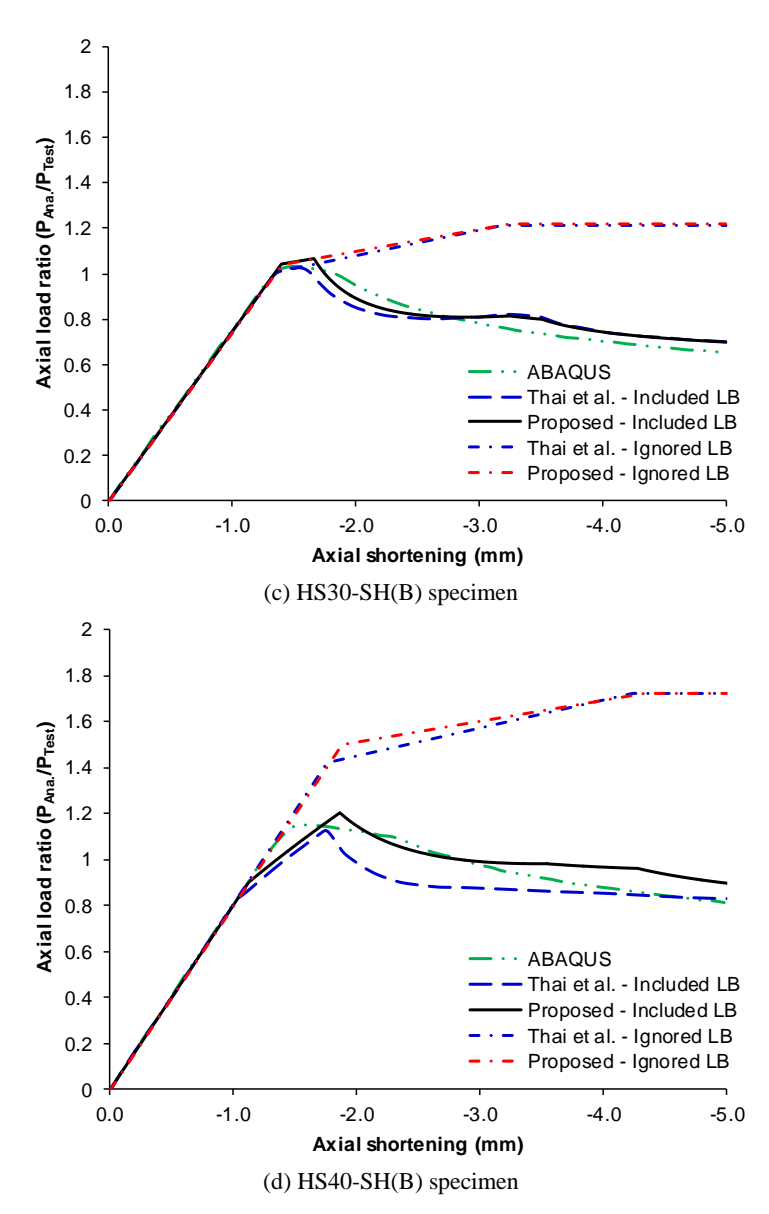


Figure 9. Load ratio-axial shortening curves of steel box stub columns with high strength

Table 6. Comparison of ultimate compression load ratios for high-strength steel box specimens

Specimens	P <sub>Test</sub> (kN)	P <sub>Ana</sub> /P <sub>Test</sub>						
	[40]	ABAQUS [10]	Thai [10] (with LB)	Thai [10] (without LB)	Present (with LB)	Present (without LB)		
HS20-SH(B)	1544	0.980	1.034	1.034	0.935	0.940		
HS25-SH(B)	1740	0.984	0.996	1.042	1.032	1.054		
HS30-SH(B)	1820	1.030	1.021	1.211	1.066	1.217		
HS40-SH(B)	1728	1.150	1.125	1.715	1.204	1.724		

# 5. Conclusion

This study successfully developed a displacement-based fiber beam-column finite element model for analyzing the nonlinear local buckling of steel stub columns under axial compression. The model incorporates two novel stress-strain relationships for compact and slender sections, utilizing a strain energy method to capture inelastic and elastic post-buckling behaviors. By integrating stability functions, the model accurately accounts for geometric nonlinearity (P– $\delta$  effects) using one-element modeling per member, as validated through numerical examples. Comparisons with experimental data and finite element analyses demonstrate the reliability of the proposed stress-strain relationships, with ultimate load ratios within 2–7% for compact sections (e.g., HI1–HI2, HS20–HS30) and 5–7% for slender sections (e.g., HB3, HS40). The model's ability to tune post-buckling behavior via the coefficient  $\alpha$  enhances its accuracy, particularly for compact sections, offering a robust alternative to traditional multi-element approaches.

The proposed model achieves significant computational efficiency, requiring approximately 1.0 second per analysis compared to an estimated 20–30 minutes for ABAQUS shell element models (Section 4.1), making it highly suitable for practical engineering design. Numerical examples highlight the critical role of local buckling, which can lead to sudden structural collapse, and the influence of residual stresses, reducing compressive strength by up to 14.4% for HB3, 63.3% for HI4, 43.2% for HS40-SH(B). It can be seen that we cannot ignore the effects of residual stress on the local buckling in the case of slender sections. The model's flexibility supports extensions to nonlinear inelastic analysis of steel frames and concrete-filled steel tube frames, incorporating local buckling effects for real-world applications. Future work could enhance accuracy for slender sections by including initial geometric imperfections, further broadening the model's applicability in structural engineering practice.

#### 6. Declarations

#### 6.1. Author Contributions

Conceptualization, P.C.N. and T.T.T.; methodology, H.P.N. and T.D.T.; formal analysis, P.C.N.; writing—original draft preparation, P.C.N., T.T.T., H.P.N., and T.D.T.; writing—review and editing, P.C.N., T.T.T., H.P.N., and T.D.T.; visualization, P.C.N. and T.T.T. All authors have read and agreed to the published version of the manuscript.

## **6.2. Data Availability Statement**

The data presented in this study are available in the article.

#### 6.3. Funding and Acknowledgements

The authors gratefully acknowledge the financial support granted by the Scientific Research Fund of the Ministry of Education and Training (MOET), Vietnam. (No. B2023–MBS–03).

#### 6.4. Conflicts of Interest

The authors declare no conflict of interest.

#### 7. References

- [1] Zhang, J., Su, A., & Yang, H. (2025). Local buckling behavior and bearing capacity of cold-formed S700 high strength steel built-up box-section stub columns. Thin-Walled Structures, 216. doi:10.1016/j.tws.2025.113590.
- [2] Schreiber, P., & Mittelstedt, C. (2025). Experimental and analytical investigation of the local buckling behaviour of unsymmetrically laminated thin-walled beams. Composite Structures, 363. doi:10.1016/j.compstruct.2025.119073.
- [3] Chen, S., Liu, J.-Z., & Chan, T.-M. (2024). Local Buckling Behavior of Hybrid Steel I-Sections under Uniform Bending: Moment-Rotation Characteristic. Journal of Structural Engineering, 150(11), 04024162. doi:10.1061/jsendh.steng-13401.
- [4] Xue, Q., Xu, S., Li, A., & Wang, Y. (2024). Local—overall buckling behavior of corroded intermediate compression-bending H-section steel columns. Engineering Structures, 308. doi:10.1016/j.engstruct.2024.118025.
- [5] Wu, K., Zhou, X., Huang, C., Xing, Z., Lu, Z., & Quan, K. (2025). Stability of prestressed stayed I-section steel columns: Zones-based and intelligent design considering local buckling. Thin-Walled Structures, 213, 113269. doi:10.1016/j.tws.2025.113269.
- [6] Zhong, Y., Jiang, K., Chen, M. T., Su, A., & Zhao, O. (2025). Local buckling of stainless steel stub columns with novel octagonal hollow sections. Engineering Structures, 338. doi:10.1016/j.engstruct.2025.120512.
- [7] Han, X., Jia, C., Hu, Q., Liu, C., & Xiang, T. (2025). Local-global buckling behaviours of axially compressive welded I-section steel columns with local corrosion. Thin-Walled Structures, 212, 113239. doi:10.1016/j.tws.2025.113239.
- [8] Yuan, W. B., Shen, Y. T., Yu, N. T., & Bao, Z. S. (2019). An Analytical Solution of Local—Global Interaction Buckling of Cold-Formed Steel Channel-Section Columns. International Journal of Steel Structures, 19(5), 1578-1591. doi:10.1007/s13296-019-00232-4.
- [9] Kolwankar, S., Kanvinde, A., Kenawy, M., Lignos, D., & Kunnath, S. (2020). Simulating Cyclic Local Buckling–Induced Softening in Steel Beam-Columns Using a Nonlocal Material Model in Displacement-Based Fiber Elements. Journal of Structural Engineering, 146(1), 04019174. doi:10.1061/(asce)st.1943-541x.0002457.
- [10] Thai, H. T., Uy, B., & Khan, M. (2015). A modified stress-strain model accounting for the local buckling of thin-walled stub columns under axial compression. Journal of Constructional Steel Research, 111, 57–69. doi:10.1016/j.jcsr.2015.04.002.
- [11] Maity, A., Kanvinde, A., Heredia Rosa, D. I., de Castro e Sousa, A., & Lignos, D. G. (2025). Simulating Interactive Buckling in Steel Members Using a Torsional Fiber Element Integrated with a Multiaxial Local Buckling Constitutive Model. Journal of Structural Engineering, 151(9), 04025124. doi:10.1061/jsendh.steng-14023.

- [12] Heredia Rosa, D. I., de Castro e Sousa, A., Lignos, D. G., Maity, A., & Kanvinde, A. (2025). A Multiaxial Plasticity Model with Softening for Simulating Inelastic Cyclic Local Buckling in Steel Beam Columns Using Fiber Elements. Journal of Structural Engineering, 151(7), 04025088. doi:10.1061/jsendh.steng-14262.
- [13] Feng, R., Chen, L., Chen, Z., Chen, B., Roy, K., & Lim, J. B. P. (2021). Nonlinear behaviour and design of stainless steel hybrid tubular K-joints with SHS-to-CHS. Journal of Constructional Steel Research, 183. doi:10.1016/j.jcsr.2021.106704.
- [14] Roy, K., Ho Lau, H., Ahmed, A. M. M., & Lim, J. B. P. (2021). Nonlinear behavior of cold-formed stainless steel built-up box sections under axial compression. Structures, 30, 390–408. doi:10.1016/j.istruc.2020.12.058.
- [15] Ananthi, G. B. G., Roy, K., & Lim, J. B. P. (2021). Tests and Finite Element Modelling of Cold-Formed Steel Zed and Hat Section Columns Under Axial Compression. International Journal of Steel Structures, 21(4), 1305–1331. doi:10.1007/s13296-021-00504-y.
- [16] Fang, Z., Roy, K., Chen, B., Xie, Z., & Lim, J. B. P. (2022). Local and distortional buckling behaviour of aluminium alloy back-to-back channels with web holes under axial compression. Journal of Building Engineering, 47. doi:10.1016/j.jobe.2021.103837.
- [17] ABAQUS. (2014). Analysis User's Manual, Version 6.14. Dassault Systemes Simulia, Inc., Waltham, United States.
- [18] Uy, B. (1998). Local and post-local buckling of concrete filled steel welded box columns. Journal of Constructional Steel Research, 47(1–2), 47–72. doi:10.1016/S0143-974X(98)80102-8.
- [19] Kim, S. E., Lee, J., & Park, J. S. (2003). 3-D second-order plastic-hinge analysis accounting for local buckling. Engineering Structures, 25(1), 81–90. doi:10.1016/S0141-0296(02)00122-0.
- [20] Kim, S. E., & Lee, J. (2002). Improved refined plastic-hinge analysis accounting for lateral torsional buckling. Journal of Constructional Steel Research, 58(11), 1431–1453. doi:10.1016/S0143-974X(01)00068-2.
- [21] Chan, S. L., Kitipornchai, S., & Al-Bermani, F. G. A. (1991). Elasto-Plastic Analysis of Box-Beam-Columns Including Local Buckling Effects. Journal of Structural Engineering, 117(7), 1946–1962. doi:10.1061/(asce)0733-9445(1991)117:7(1946).
- [22] Skallerud, B., & Amdahl, J. (1998). Modelling methodologies with beam finite elements for collapse analysis of tubular members/cylindrical shells. Proceedings of the 2<sup>nd</sup> International Conference on Thin-Walled Structures, 2–4 December, 1998, Singapore.
- [23] Skallerud, B., Amdahl, J., Johansen, A., & Eide, O. I. (1996). Cyclic capacity of tubular beam-columns with local buckling: numerical and experimental studies. 15<sup>th</sup> International Conference on Offshore Mechanics and Arctic Engineering (OMAE 1996), 16-21 June, 1996, Florence, Italy.
- [24] Neuenhofer, A., & Filippou, F. C. (1998). Geometrically Nonlinear Flexibility-Based Frame Finite Element. Journal of Structural Engineering, 124(6), 704–711. doi:10.1061/(asce)0733-9445(1998)124:6(704).
- [25] De Souza, R. M. (2000). Force-based finite element for large displacement inelastic analysis of frames. Ph.D. Thesis, University of California, Berkeley, United States.
- [26] Yang, Y. Bin, & Shieh, M. S. (1990). Solution method for nonlinear problems with multiple critical points. AIAA Journal, 28(12), 2110–2116. doi:10.2514/3.10529.
- [27] Bryan, G. H. (1890). On the stability of a plane plate under thrusts in its own plane, with applications to the buckling of the sides of a ship. Proceedings of the London Mathematical Society, s1-22(1), 54–67. doi:10.1112/plms/s1-22.1.54.
- [28] Lee, J. H., & Mahendran, M. (2018). Local Buckling Behaviour and Design of Cold-Formed Steel Compression Members at Elevated Temperatures. Thin-Walled Structures, 315–322, CRC Press, Boca Raton, United States. doi:10.1201/9781351077309-34.
- [29] Mursi, M., & Uy, B. (2004). Strength of slender concrete filled high strength steel box columns. Journal of Constructional Steel Research, 60(12), 1825–1848. doi:10.1016/j.jcsr.2004.05.002.
- [30] Chen, W.F., & Lui, E.M. (1987). Structural Stability: Theory and Implementation, Elsevier, New York, United States.
- [31] Nguyen, P. C., & Kim, S. E. (2013). Nonlinear elastic dynamic analysis of space steel frames with semi-rigid connections. Journal of Constructional Steel Research, 84, 72–81. doi:10.1016/j.jcsr.2013.02.004.
- [32] Nguyen, P. C., & Kim, S. E. (2014). Nonlinear inelastic time-history analysis of three-dimensional semi-rigid steel frames. Journal of Constructional Steel Research, 101, 192–206. doi:10.1016/j.jcsr.2014.05.009.
- [33] Nguyen, P. C., & Kim, S. E. (2014). An advanced analysis method for three-dimensional steel frames with semi-rigid connections. Finite Elements in Analysis and Design, 80, 23–32. doi:10.1016/j.finel.2013.11.004.
- [34] Nguyen, P. C., & Kim, S. E. (2015). Second-order spread-of-plasticity approach for nonlinear time-history analysis of space semi-rigid steel frames. Finite Elements in Analysis and Design, 105, 1–15. doi:10.1016/j.finel.2015.06.006.

- [35] Nguyen, P. C., & Kim, S. E. (2017). Investigating effects of various base restraints on the nonlinear inelastic static and seismic responses of steel frames. International Journal of Non-Linear Mechanics, 89, 151–167. doi:10.1016/j.ijnonlinmec.2016.12.011.
- [36] Nguyen, P. C., & Kim, S. E. (2018). A new improved fiber plastic hinge method accounting for lateral-torsional buckling of 3D steel frames. Thin-Walled Structures, 127, 666–675. doi:10.1016/j.tws.2017.12.031.
- [37] Michels, H. H. (1963). Abscissas and Weight Coefficients for Lobatto Quadrature. Mathematics of Computation, 17(83), 237. doi:10.2307/2003841.
- [38] Kitipornchai, S., & Wong- Chung, A. D. (1987). Inelastic Buckling of Welded Monosymmetric I-Beams. Journal of Structural Engineering, 113(4), 740–756. doi:10.1061/(asce)0733-9445(1987)113:4(740).
- [39] Uy, B. (2001). Local and Postlocal Buckling of Fabricated Steel and Composite Cross Sections. Journal of Structural Engineering, 127(6), 666–677. doi:10.1061/(asce)0733-9445(2001)127:6(666).
- [40] Uy, B., Khan, M., Tao, Z., & Mashiri, F. (2013). Behaviour and design of high strength steel-concrete filled columns. Proceedings of the 2013 world congress on advances in structural engineering and mechanics (ASEM13), 8-12 September, 2013, Jeju, Korea.